

Joint carrier frequency and phase offset estimation algorithm for CPM-DSSS based secure point-to-point communication

Saima SHEHZADI^{1,*}, Farzana KULSOOM², Muhammad ZEESHAN¹,
Qasim Umar KHAN¹, Shahzad Amin SHEIKH¹

¹Department of Electrical Engineering, College of Electrical and Mechanical Engineering,
National University of Science and Technology, Islamabad, Pakistan

²Department of Telecommunication Engineering, University of Engineering and Technology, Taxila, Pakistan

Received: 01.05.2021

Accepted/Published Online: 26.10.2021

Final Version: 30.11.2021

Abstract: A point-to-point (P2P) communication system based on the CPM-DSSS scheme ensures reliability, security, and antijamming capabilities. However, for reliable detection of data carrier synchronization of CPM-DSSS based system is one of the requirements. This paper presents a joint algorithm for carrier frequency offset (CFO) and carrier phase offset (CPO) estimation for CPM-DSSS based P2P system. The results indicate that the proposed CFO estimator is unbiased and can accurately estimate a wide range of offsets. Moreover, the proposed algorithm is compared with another research work. The results show that the proposed CFO and CPO estimation algorithm outperforms its counterpart with a performance improvement of about 9 dB and above, respectively. The effectiveness of the proposed estimator in the Stanford University Interim (SUI)-1 multipath fading channel is also demonstrated. Finally, the proposed estimator's bit-error-rate (BER) performance and computational complexity are also given for the CPM-DSSS P2P system.

Key words: Carrier frequency offset, wideband CPM-DSSS waveform of software defined radio, carrier synchronization, carrier phase offset, point-to-point communication

1. Introduction

Point-to-point (P2P) communication is an essential component of the modern wireless communication system. Typical examples of P2P systems are device-to-device (D2D), machine-to-machine (M2M), and vehicle-to-vehicle (V2V) communication. P2P is employed in several fields, such as military systems, 5G mobile communication to improve the spectral efficiency and off shed load in cellular systems [1]. The general requirements of P2P systems are a high level of reliability, throughput, spectral efficiency, and infallible security. Particularly the military-based systems demand a higher level of security. One of the use cases of such security for military applications is antijamming (AJ). The AJ provides a capability to the radio communication system to prevent itself from being blocked or disrupted from external sources [2, 3]. Another important security requirement is evading a middle party to eavesdrop on the communication link.

AJ capabilities are achieved in the literature by employing frequency hopping spread spectrum (FHSS) or direct sequence spread spectrum (DSSS). In FHSS, the spectrum is split into distinct frequency bands, and the carrier frequency rapidly hops between these specific frequency bands. Contrary to that, in the case of DSSS, the data bits are first encoded, and then they are spread over the full spectrum. However, due to

*Correspondence: saima.shahzadi@ceme.nust.edu.pk

frequency hopping, FHSS becomes an expensive solution than DSSS [4]. Although both FHSS and DSSS are spread-spectrum techniques with AJ capabilities, they can not efficiently utilize the available spectrum. For attaining better spectrum efficiency and high throughput, orthogonal frequency division multiplexing (OFDM) has been established as one of the very famous techniques. But it has other problems, for example, sensitivity to Doppler shift and to the carrier frequency and phase offset (CFO and CPO); further, it is more prone to security threats. Therefore, the spreading technique like FHSS is primarily applied in literature with the OFDM system to achieve spectral efficiency and antijamming. Besides that, FHSS-OFDM based systems are more suitable for optimal power utilization, which is a critical requirement in battery-held devices. Apart from all benefits of FHSS, it has various issues, including synchronization, frequency hopping, and reconnections. On top of that, the FHSS-OFDM system is susceptible to disguised jamming scenarios [5]. On the other hand, DSSS based systems are not sensitive to CFO and CPO, and it does not require time and other resources for frequency hopping; hence it is fast and computationally more efficient than FHSS based systems. Because of better processing capabilities, it also has higher throughput. Nevertheless, the DSSS based system suffers from high power consumption, and this scheme does not utilize spectrum efficiently. A joint scheme based on CPM and DSSS can combat the problems mentioned earlier. For example, the combination of CPM-DSSS has higher antijamming capabilities due to a lower probability of interception. Moreover, the CPM offers a constant envelope useful for nonlinear amplifiers that are much more cost-effective [6]. CPM-DSSS based system is also more efficient at higher frequencies as compared to FHSS based system [7]. Thanks to the CPM-based system's narrow power spectrum density (PSD), it offers a much higher processing gain and an efficient matched filter design. The higher processing gains result in a better capability to mitigate interference [8].

The frequency and phase of the signal are affected as the signal travels over the noisy and non-ideal channel. The two primary problems include CFO and CPO, which result in distortion of frequency and phase of the received signal. The primary reason for CFO is frequency mismatch between transmitter and receiver oscillators. The relative motion of the transmitter and receiver, also known as Doppler's effect, is another factor for CFO. Furthermore, CPO results from a lack of carrier's phase knowledge of the transmitter's oscillator at the receiver. Therefore, for reliable data reception at the receiver, CPO and CFO must be estimated and compensated accurately. The CPM-DSSS, as a suitable AJ scheme, similar to other communication systems is also affected by CFO and CPO. There are numerous schemes for the estimation of CFO in the literature for variants of CPM based systems. The methods in [9–11] are suitable for burst mode transmission, nondata-aided and consist of a feed-forward structure. The techniques presented in [9] and [10] can compensate the frequency offsets up to 25% of data rate. However, [9] is only appropriate for CFO estimation for minimum shift keying (MSK) based systems while [10] supports both MSK and gaussian MSK (GMSK) based modulations. Furthermore, the algorithm in [11] presents a joint estimation of symbol timing and frequency offset, which is suitable for both MSK and GMSK. For MSK, it can estimate the frequency offset 25% of the data rate, while for GMSK, it can estimate the frequency offset 15% of data rate. However, at low SNR, the techniques in [9–11] perform poorly in terms of mean square error (MSE). Another work [12, 13] is data-aided (DA), maximum likelihood (ML), and feed-forward algorithm for synchronization of burst mode CPM. This algorithm is designed for optimum training sequence, it can jointly estimate the frequency offset, symbol timing, and carrier phase [14]. The estimator's variance in this case approaches the Cramer-Rao bound (CRB) for the synchronization parameters at SNRs as low as 0 dB. However, the algorithm in [12] is limited to the burst mode CPM and is unsuitable for estimating CFO and CPO for the CPM-DSSS based systems. The fundamental reason is based on the fact that in CPM-DSSS, the training sequence and data have to undergo spreading before CPM modulation. This

breaks the training sequence's optimum structure, and the spread training sequence does not minimize the CRB for all synchronization problems any longer. A two-stage algorithm for CFO estimation employing burst mode transmission compatible with standard DSSS based software-defined radio (SDR) waveform was presented in [15]. The algorithm can estimate the considerable frequency offsets, and the MSE performance of the estimator approaches the CRB at high SNRs. The estimation of CFO, CPO, fractional timing offset estimation and frame synchronization for MSK-DSSS system specifically for wireless sensor networks is presented in [16]. The work in this paper is quite different from our proposed work as they are using separate algorithms for estimation of each of the above mentioned parameters for example, CFO in that paper is estimated using DFT operation and CPO by least square (LS) estimator whereas we have used ML algorithm for joint estimation CFO and CPO. Although the work presented in [17] and the current work are both based on the CPM-DSSS system; however, both are different in terms of estimation of synchronization parameters as well as phase response approximations. Firstly, in [17], the timing and phase offsets are estimated and compensated by assuming the ideal frequency synchronization; on the contrary, in this work, phase and frequency are estimated by assuming perfect timing synchronization. Secondly, the phase response of raised-cosine and Gaussian pulse is approximated with rectangular pulse phase response while in the current work, the actual phase response of the frequency pulse is considered. Thus, we conclude that the joint estimation of CFO and CPO using ML algorithm is not yet reported in the literature for CPM-DSSS based P2P communications. Our main contributions are listed as follows:

- A novel maximum likelihood, data-aided algorithm for the joint estimation of CFO and CPO is presented for the CPM-DSSS scheme.
- The effectiveness of the proposed algorithms is also tested in SUI-1 multipath channel.

Figure 1 demonstrates the system flow diagram for the estimation of CFO and CPO, considering the CPM-DSSS scheme for a general P2P communication system. As can be seen, a burst is formed by inserting a training sequence at the start of the payload, which carries the information symbols. In this work, training sequence used is inspired from [12–14] for burst mode CPM system. The carrier generated from the reference oscillator modulates the CPM-DSSS burst and passes it to the channel. The receiver's crystal oscillator instability will produce the phase and frequency offset [18, 19]. Which will results in overall system performance degradation. The organization of the rest of the paper is as follows: Section 2 covers system overview and model, Section 3 provides the proposed joint estimation algorithm, Section 4 presents the results and discussion part and Section 5 concludes the paper.

2. System overview and model

This section presents the system overview and model for a CPM-DSSS scheme. As shown in Figure 1, first, the data stream is passed through M -pulse amplitude modulation (M -PAM) encoding block at the transmitter side. Where, M is the alphabet size and its value is lies in the set $\{-(M-1), \dots, -3, -1, 1, 3, \dots, (M-1)\}$. The $M = 2$ is considered in this paper i.e. 2-PAM is used therefore the alphabets values will be from the set $\{-1, 1\}$. Next, the 2-PAM encoded training sequences are placed before each of the encoded data symbols to form the bursts of the symbols in the framing block. Subsequently these bursts are spread using the DSSS technique and fed to the CPM block. The CPM block's output is CPM-DSSS burst. The carrier generated from the reference oscillator modulates this burst and passes it to the channel. At the receiving end, the crystal oscillator produces CFO and CPO. Assuming perfect time synchronization, these offsets are estimated at the

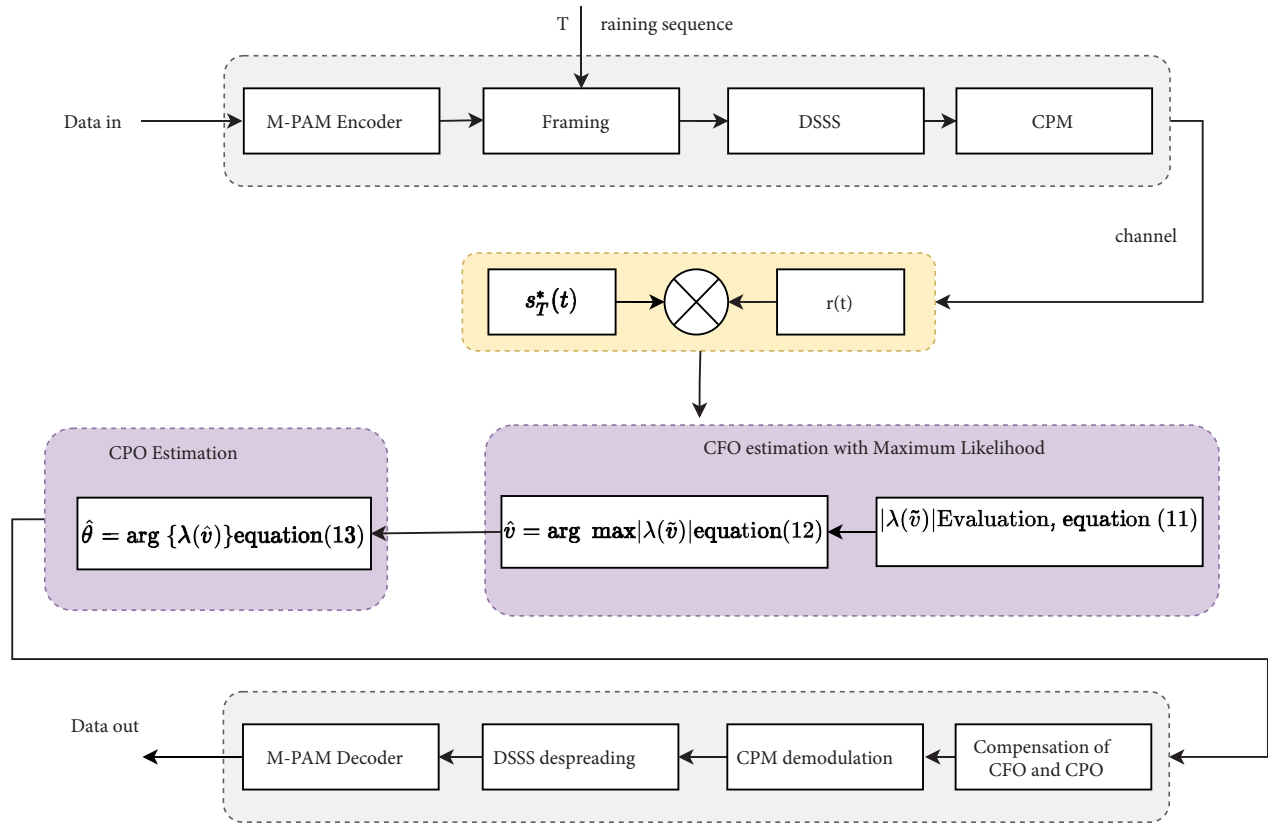


Figure 1. CFO and CPO estimation system flow diagram.

digital front end using the proposed joint estimation algorithm to be presented in Section 3 and ultimately compensated. The estimation and compensation block’s output is passed through the CPM demodulator block followed by despreading operation. Lastly, M-PAM decoding is performed to retrieve the original data stream.

2.1. CPM-DSSS signal model

In this model, transmission of bursts is considered. The duration and structure of the burst is known at the receiver, which consists of two parts. The first part is the training sequence or synchronization preamble and second part is the payload. The training sequence or synchronization preamble consists of L_0L_c chips which are used to estimate CFO and CPO. Where, L_0 is the length of preamble before spreading and L_c is the length of spreading sequence. In our case, Golay complementary sequence [20, 21] of length $L_c = 8$ is used as spreading sequence. Thus the duration of training sequence of the burst, before passing to the CPM block, is $T'_0 = L_0L_cT_c$. Please note that the spreading block maps each symbol in the unspread burst of length L_0 to chips called α_i using the spreading sequence of length L_c , where α_i is the sequence of 2-ary chip sequence selected from the set of $\{-1, 1\}$. Thus, the CPM phase function [8] for the spread form of synchronization preamble is given as:

$$\varphi(t, \alpha) = 2\pi h \sum_{i=0}^{L_cL_0-1} \alpha_i q(t - iT_c), \tag{1}$$

where $q(t)$ is given as integral of some pulse $g(t)$ with the duration of LT_c i.e. $q(t) = \int_0^t g(\tau)d\tau$ and is also called phase response of CPM. The CPM signal is called the full response signal when $L = 1$ and it is referred to as partial response signal when $L > 1$. In this work, the Gaussian pulse is used as the pulse $g(t)$ and the bandwidth-time (BT) product of pulse is set to 0.3. The h in Equation (1) is termed as modulation index, and its value is assumed to be 0.5 in our case. In other words the parameters of GMSK, which is one of the variant of the CPM modulation scheme, is considered. The reason for choosing Gaussian pulse as the pulse $g(t)$ for CPM-DSSS burst is that the spectral efficiency of GMSK is higher while compared with other $g(t)$ pulses i.e. rectangular (REC), root raised cosine (RRC), raised cosine (RC) etc. used with CPM. Moreover, GMSK is widely employed in GSM, DECT, and wireless communications where economical class C amplifiers can be used due constant envelope of the GMSK signal. Apart from that, the BT product is assumed as an important parameter of GMSK as it is observed in [22] that a decrease in bandwidth causes the duration of Gaussian pulse to increases which propel higher intersymbol interference (ISI). Hence, there exists a tradeoff between tolerable ISI and bandwidth occupancy while choosing the value of BT product. As stated earlier, the value BT product is 0.3 which is the value used by GSM as well, thus providing us confidence in our choice of value through its efficiency. Now, the complex baseband CPM-DSSS signal for the span of the synchronization preamble can be written as:

$$s_T(t) = e^{j\varphi(t,\alpha)}. \quad (2)$$

Now the received baseband signal $r(t)$ for the time length of training sequence after passing through the AWGN channel is expressed as:

$$r(t) = e^{j(2\pi f_d t + \theta)} s_T(t) + w(t), \quad (3)$$

where θ is unknown CPO, f_d is the unknown CFO and $w(t)$ represents the complex baseband additive white Gaussian noise (AWGN) with mean zero and PSD N_0 .

3. The proposed joint estimation algorithm

The precise knowledge of CFO and CPO is required for the reliable detection of CPM-DSSS signal. In this work, while assuming perfect timing synchronization, we apply joint ML algorithm for estimating CFO and CPO in which the spread training sequence, α , is known to the receiver. The joint log-likelihood function (LLF) for estimating CFO and CPO in our problem i.e. when the signal is complex and constant envelope is expressed [12, 13] within a constant factor of Equation (4).

$$\Lambda(r(t); \tilde{f}_d, \tilde{\theta}) = \text{Re} \left[\int_0^{T'_0} e^{-j(2\pi \tilde{f}_d t + \tilde{\theta})} r(t) s_T^*(t) dt \right], \quad (4)$$

where $\tilde{\theta}$ and \tilde{f}_d represents the trial values for the CPO and CFO respectively and T'_0 is spread training sequence duration. The ML criterion requires that one must choose those trial values of f_d and θ as the ML estimates which maximizes equation (4). The ML estimates for CFO and CPO are denoted as \hat{f}_d , $\hat{\theta}$. Now, rearranging Equation (4) as follows:

$$\Lambda(r(t); \tilde{f}_d, \tilde{\theta}) = \text{Re} \{ e^{-j\tilde{\theta}} \int_0^{T'_0} e^{-j(2\pi \tilde{f}_d t)} r(t) s_T^*(t) dt \}. \quad (5)$$

Further, Equation (5) can be expressed by denoting the terms corresponding to CFO as $\lambda(\tilde{f}_d)$

$$\Lambda(r(t); \tilde{f}_d, \tilde{\theta}) = \text{Re} \left[e^{-j\tilde{\theta}} \lambda(\tilde{f}_d) \right], \quad (6)$$

where

$$\lambda(\tilde{f}_d) = \int_0^{T_0'} e^{-j(2\pi\tilde{f}_d t)} r(t) s_{\text{T}}^*(t) dt. \quad (7)$$

It can be observed that for any trial values of \tilde{f}_d LLF in Equation (6) is maximized by choosing θ such that it rotates $\lambda(\tilde{f}_d)$ towards the real axis i.e.

$$\tilde{\theta} = \arg\{\lambda(\tilde{f}_d)\} \quad (8)$$

which reduces LLF to $|\lambda(\tilde{f}_d)|$ as described in [12, 13]. Now maximization of LLF results in the ML estimate of CFO i.e. \hat{f}_d which is mathematically expressed as follows:

$$\hat{f}_d = \arg \max_{\tilde{f}_d} |\lambda(\tilde{f}_d)| \quad (9)$$

once the CFO is estimated from equation (9) the ML estimates for CPO is obtained by using equation (8) as

$$\hat{\theta} = \arg\{\lambda(\hat{f}_d)\}. \quad (10)$$

The channel is producing rotation in the constellation which is compensated by rotating back the constellation by the estimated value in opposite direction i.e. using Equation (17).

3.1. Implementation of the proposed joint estimation algorithm

In the previous section, continuous-time functions and integral are considered while describing the proposed joint estimation method. We will now discretize the received signal $r(t)$ by sampling it at rate of N times per chip interval T_c . As a consequence, the sampled received signal becomes $r[i] = r(iT_c/N)$. Further, we normalize CFO with sampling frequency, i.e. $v = f_d T_c / N$. Thus, the discrete-time version of Equation (7) can be given as:

$$\lambda(\tilde{v}) = \sum_{i=0}^{L_0 L_c N - 1} r(i) \cdot s_{\text{T}}^*(i) e^{-j2\pi i \tilde{v}}. \quad (11)$$

The \tilde{f}_d in Equation (7) has been replaced by v in Equation (11) in order to find the normalized frequency offset. Thus after discretization and normalization Equation (9) will become:

$$\hat{v} = \arg \max_{\tilde{v}} |\lambda(\tilde{v})|. \quad (12)$$

Similarly, Equation (10) for CPO estimate can be rewritten as;

$$\hat{\theta} = \arg\{\lambda(\hat{v})\}. \quad (13)$$

It must be noted that our proposed joint estimator is different from the estimator in [12, 13] in the following ways: Firstly, the algorithm in [12, 13] is based on an optimum training sequence with a specific phase trajectory.

Whereas the proposed algorithm for the CPM-DSSS system uses a more generic approach, i.e. it can be used with any other training sequence for CPM modulation in the literature. Also, in [12, 13] the training sequence of duration L_0T_s is modulated directly with the CPM scheme. Whereas for the CPM-DSSS system, the training sequence of length L_0 is first spread using DSSS with spreading code of length L_c , then modulates using the CPM scheme. This can be understood from the phase-response equations of both system. For example, for the CPM system, the phase-response equation for the duration of training sequence L_0T_s is given as

$$\varphi(t, \gamma) = 2\pi h \sum_{i=0}^{L_0-1} \gamma_i q(t - iT_s), \quad (14)$$

where T_s is the symbol duration. Now, the phase response for CPM-DSSS scheme for the duration of spread form of training sequence $L_0L_cT_c$ is given in Equation (1). Please note that the $T_c = \frac{T_s}{G}$, where G is the spreading gain i.e. $T_c \ll T_s$. The G in our case is equal to spreading sequence length L_c .

Lastly, in [12, 13] the phase response is approximated with full response REC pulse phase response when considering a different type of pulses $g(t)$, i.e. RC and Gaussian pulses. Whereas for the proposed estimation algorithm, the actual phase response of the pulse $g(t)$, i.e. Gaussian pulse, is considered.

Now, the calculation of Equation (11) for different values of \tilde{v} look like the discrete Fourier transform (DFT) operation where \tilde{v} is replaced by trial values of discrete frequencies. Generally, the fast Fourier transform (FFT) algorithm performs the DFT operations efficiently. Thus the size of FFT in Equation (11) will be equal to the summation length L_0L_cN . Where the trial values used in Equation (11) in order to find the closest CFO estimate are $\tilde{v} \in [0, 1/L_0L_cN, \dots, (L_0L_cN - 1)/L_0L_cN]$. The CFO estimation performance is limited by the resolution of the FFT operations which refers to the distance between the discrete frequency components. Therefore the the frequency estimation accuracy can be improved by employing two approaches. In the first approach the FFT operands are zero padded in Equation (11) such that the size of FFT is $K_zL_0L_cN$; where K_z is zero padding factor which is power of 2. In the second approach an interpolator is to applied to find the true maximum of Equation (12) between the discrete frequency components. This algorithm utilizes the quadratic interpolator presented in [23] which can be expressed as follows:

$$\hat{v} = \hat{v}_m + \frac{1}{2} \frac{(h_{m-1} - h_{m+1})}{(h_{m-1} - 2h_m + h_{m+1})} v_{\text{resolution}}, \quad (15)$$

where \hat{v}_m in Equation (15) represents the maximizing frequency resulting from equation (9) and h_m represents energy at this frequency i.e. \hat{v}_m . The h_{m-1} and h_{m+1} represents the energies at the point \hat{v}_{m-1} and \hat{v}_{m+1} which in terms of FFT operation represents the discrete frequency values before and after \hat{v}_m , respectively. Also, the FFT frequency resolution is given as $v_{\text{resolution}} = \hat{v}_m - \hat{v}_{m-1}$. Thus the fine CFO estimates search operation is performed in equation (15) while a coarse search is performed in Equation (12). Once the CFO is estimated, next step is to find the CPO according to Equation (13). Note that the FFT operations are periodic with NL_0L_c period. The negative frequency offsets can be represented by the values of $\frac{1}{2} \leq \tilde{v} < 1$ and hence \tilde{v} is estimated for $[-0.5, 0.5)$. With this the frequency estimation range is limited to

$$-\frac{N}{2T_c} \leq \hat{f}_d < \frac{N}{2T_c}. \quad (16)$$

Therefore, by increasing the sampling frequency, the estimation range can be increased. The proposed algorithm can work efficiently in applications where the CFO is greater than the chip rate. After the estimation of CFO

from Equation (12) and CPO from Equation (13) received data is compensated by following Equation as given in [15]

$$r_c[i] = r[i]e^{-j(2\pi\hat{\nu}i+\hat{\theta})} \quad i = L_0L_cN + 1, \dots, L_0L_cN + B - 1 \quad (17)$$

where r is the discrete time version of received burst; B is the size of the spread burst and r_c is the data after CFO and CPO compensation.

4. Results and discussion

This section presents the simulation results of the proposed joint estimation algorithm for CPM-DSSS scheme. The simulations are carried out using MATLAB. Following parameters are used for the simulation i.e. spreading gain, $L_c = 8$, length of training sequence before spreading is $L_0 = 64$ symbols and size of burst before spreading is $M_b = 164$ symbols respectively, samples per chip are $N = 2$ and zero padding factor $K_z = 4$. Firstly, the performance of CFO estimator and then that of CPO estimator is given. Next, the variance of the proposed algorithm performance is compared with another algorithm [12] and then the BER performance of the proposed estimator in AWGN and SUI-1 multipath fading channel is compared with ideal case i.e. when CFO and CPO are known at the receiver. Finally, the section ends with the computational complexity of the proposed algorithm.

4.1. Performance of the proposed CFO estimator

4.1.1. CFO estimate vs. actual normalized CFO

In this subsection, graph of CFO estimate vs. actual normalized CFO is compared with graph of reference signal i.e. ideal behaviour of unbiased estimator. Figure 2 shows the relative CFO estimates vs. the actual normalised CFO for SNR of -10 dB and SNR of 0 dB. For this graph the actual normalized CFO ranges between $[-0.5, 0.5]$. Each point in the graphs has been obtained by taking average of 2,000 independent and random CFO estimates. It can be observed that the proposed CFO estimator is unbiased and efficiently estimates CFO throughout the specified range even for low SNR of -10 dB.

4.1.2. The proposed CFO estimator performance in AWGN and SUI-I channel

In this subsection, variance of the proposed CFO estimator in AWGN is compared with modified CRB (MCRB) and SUI-I multipath fading channel whose parametric details are as follows: path delays in μsec as $[0.0, 0.4, 0.9]$, power in (dB) as $[0.0, -15, -20]$, K-factor of 4, and maximum Doppler spread of 0.5 (Hz) [24]. The variance of any estimator [25] is given in Equation (18).

$$\text{var}(\hat{\epsilon}) = \frac{1}{M} \sum_{i=1}^M (\hat{\epsilon}_i - \hat{E}(\hat{\epsilon})), \quad (18)$$

where \hat{E} in Equation (18) is the sample mean of the estimates $\hat{\epsilon}$ which is given in Equation (19) and M is the total number of realizations used.

$$\hat{E}(\hat{\epsilon}) = \frac{1}{M} \sum_{i=1}^M \hat{\epsilon}_i \quad (19)$$

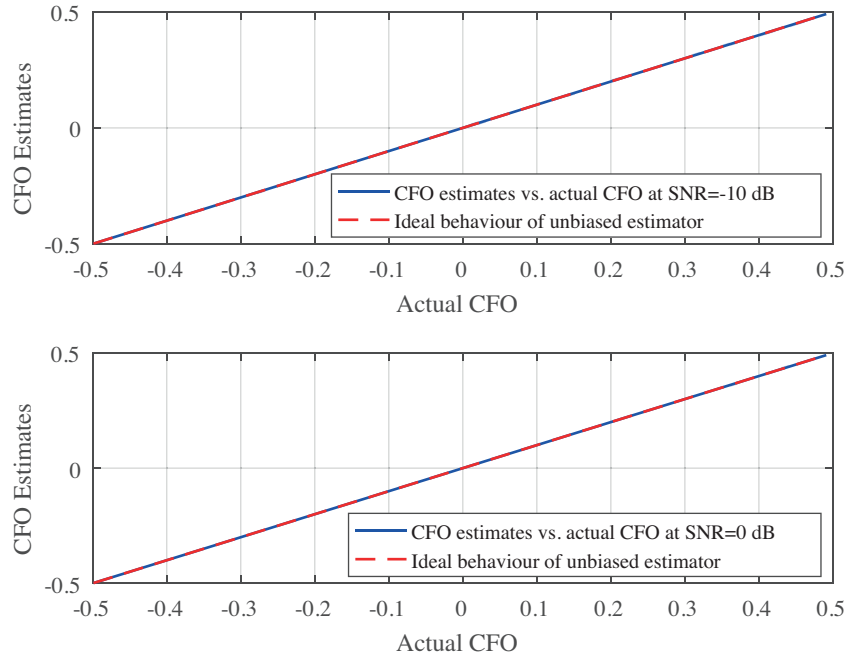


Figure 2. Relative CFO estimates vs. the actual normalised CFO for SNR of -10 dB and 0 dB.

At each SNR the normalized frequency offset is generated randomly $(-0.5, 0.5)$ and the variance of CFO estimate is averaged over $M = 2000$ statistically independent estimates.

MCRB for CFO estimates is calculated by using Equation (20) as in [26].

$$\text{MCRB}(v) = \frac{3}{8\pi^2 L_x^3 \frac{E_s}{N_0}}, \quad (20)$$

where L_x is the number of samples per symbol used for the estimation of CFO estimates where the value of this parameter is different for the CPM system and the CPM-DSSS system, E_s/N_0 is the SNR. Figure 3 depicts the variance of the proposed CFO estimator in AWGN with MCRB. Then Figure 4 compares the proposed CFO estimator's variance in AWGN with SUI-I multipath fading channel. It can be observed in Figure 3 that the proposed CFO estimator's variance is close to MCRB at all SNRs. Moreover, from Figure 4 it can be noted that although SUI-I is a multipath fading channel, still its performance is approaching to AWGN channel for almost all SNRs.

4.2. The proposed CPO estimator performance in AWGN and SUI-I channel

This subsection compares the proposed CPO estimator variance in AWGN with MCRB for phase estimation and SUI-1 multipath channel respectively. MCRB for CPO estimation is calculated by utilizing Equation (21) as given in [26].

$$\text{MCRB}(\theta) = \frac{1}{2L_x \frac{E_s}{N_0}} \quad (21)$$

Similar to CFO estimation, the phase offset is generated randomly $(0, 2\pi)$ at each SNR and the variance of the CPO estimate is averaged over $M = 2000$ statistically independent estimates. Figure 5 exhibits the comparison

of the proposed CPO estimator's variance with MCRB in the AWGN channel. It can be seen that the proposed CPO estimator variance is close to MCRB at all SNRs. Next, Figure 6 shows the comparison of variance of CPO estimator in AWGN with variance of CPO estimator in SUI-I multipath channel. As depicted in Figure 6 that the proposed CPO estimator is robust in SUI-I channel effects as well and is approaching to AWGN channel for almost all SNRs. Thus the proposed estimator is robust in multipath fading channel effects and efficiently estimate the desired parameter.

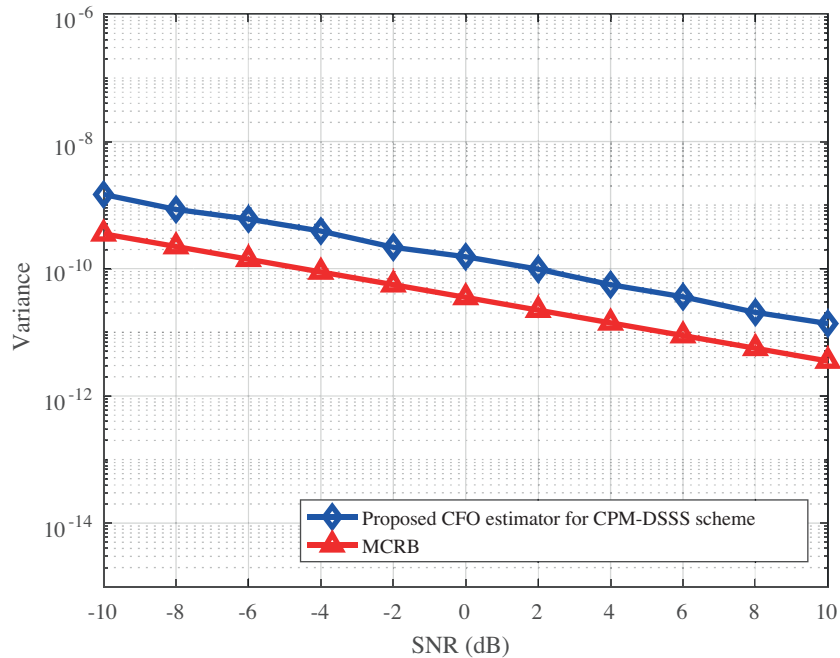


Figure 3. Variance versus SNR graph of the proposed CFO estimator with MCRB in AWGN channel for random value of CFO at each SNR.

4.3. The proposed joint estimation algorithm performance comparison with ML algorithm for CPM system

In this subsection we have compared the proposed joint algorithm for CFO and CPO estimation with another algorithm given in [12]. The comparison is depicted in terms of variance of estimator, as shown in Figures 7 and 8. It is important to mention that comparison has been done under the same simulation parametric constraints as given in [12]. For example, training sequence length, before spreading, is $L_0 = 64$ as in their case, also for the comparison purpose the value of $N = 2$, which represents the samples per symbol in case of CPM system and it represent samples per chip in case of CPM-DSSS system. Figures 7 and 8 reveal that with increase in the SNR the variance starts decreasing which indicates an improvement in CFO and CPO estimation respectively. Therefore, it is concluded from the graphs of Figures 7 Figure 8 that the proposed joint algorithm for CFO and CPO estimation is better than ML algorithm for burst mode CPM presented in [12].

4.4. BER performance of the proposed joint estimator

This subsection compares the proposed joint estimator BER performance with the case when there is perfect carrier synchronization i.e. when the receiver knows CFO and CPO. The BER performance of the proposed joint

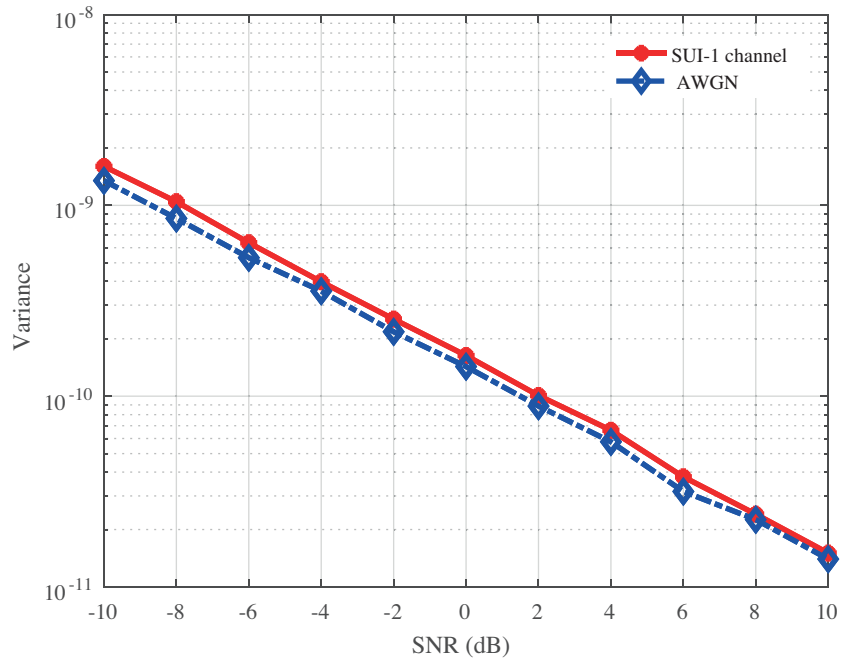


Figure 4. Comparison of variance versus SNR graph of the proposed CFO estimator in SUI-I multipath fading channel and in AWGN channel.

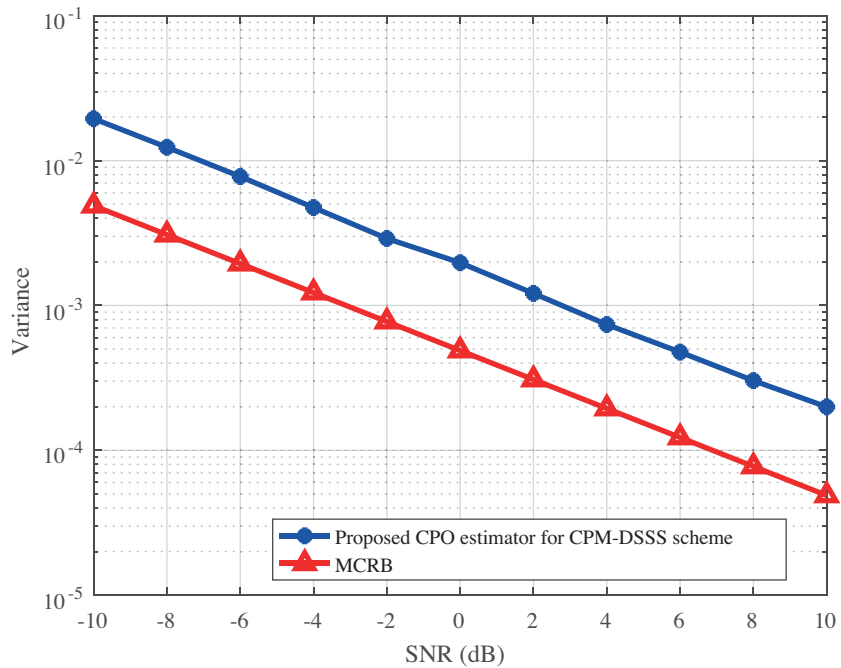


Figure 5. Variance versus SNR graph of the proposed CPO estimator with MCRB in AWGN for random values of phase offset at each SNR.

estimator with the ideal case i.e. for perfect carrier synchronization, in AWGN channel and SUI-1 multipath fading channel is shown in Figure 9. It can be observed that the system's BER performance utilizing the joint

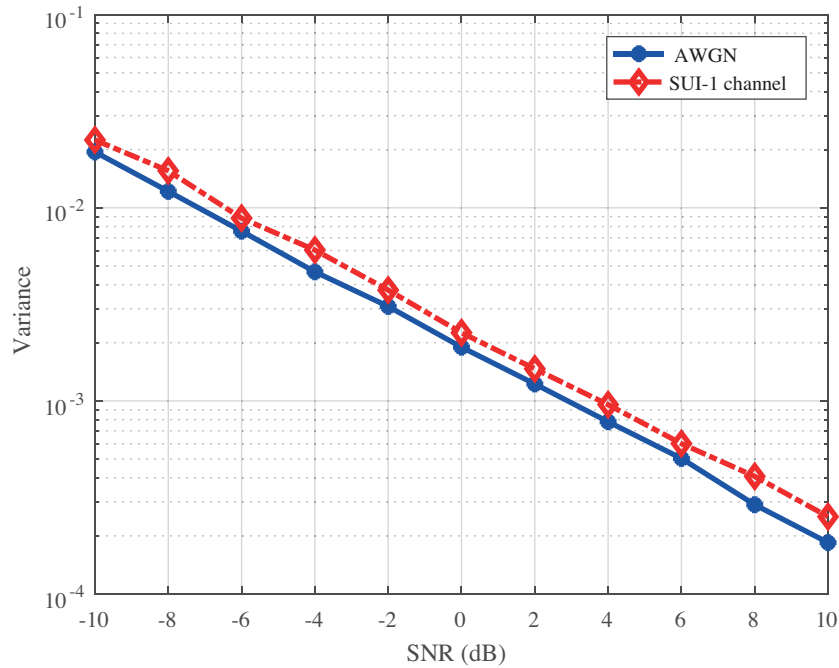


Figure 6. Performance comparison of the proposed CPO estimator in SUI-I multipath fading channel and in AWGN channel.

Table 1. Computational complexity of the proposed joint estimation algorithm.

Operation	Additions/subtractions	Multiplications/divisions
CFO estimation equation (12)	$L_0L_cN + (L_0L_cNK_z)\log_2(L_0L_cNK_z)$	$(L_0L_cNK_z/2)\log_2(L_0L_cNK_z)$
CPO estimation equation (13)	$L_cL_0NK_z - 1$	$L_cL_0NK_z + \log_2(L_cL_0NK_z + 3) + 1$
Interpolation equation (15)	5	4

estimation algorithm approaches the ideal case at all $\frac{E_b}{N_0}$ for both channels.

4.5. Computational complexity

This subsection describes the computational complexity of the proposed algorithm. The proposed joint estimation algorithm's computational complexity in terms of the number of additions/subtraction and multiplications/division for the training sequence of a single CPM-DSSS burst is given in Table 1.

The training sequence of length L_0 that has been spread using Golay code of length L_c results in a spread sequence of length L_0L_c . Subsequently, the spread sequence is CPM modulated chips, utilizing N sample per chips, which yields in the length of the transmitted training sequence as L_0L_cN .

Since, an R -point FFT requires $(R/2)\log_2(R)$ complex additions and $(R)\log_2(R)$ multiplications [27]. The equation (12), which is normalized CFO estimation equation can be used to represent CFO computational complexity. For example, for the different trial values $\tilde{v} \in [0, 1/L_0L_cN, \dots, (L_0L_cN - 1)/L_0L_cN]$ it looks like the discrete Fourier transform (DFT) operation. Thus after zero padding, the product of received training sequence r and the known training sequence signal s_T at the receiver, by a factor of K_z will produce the computational complexity of CFO estimation equation as: multiplications $\{L_0L_cN + (L_0L_cNK_z)\log_2(L_0L_cNK_z)\}$

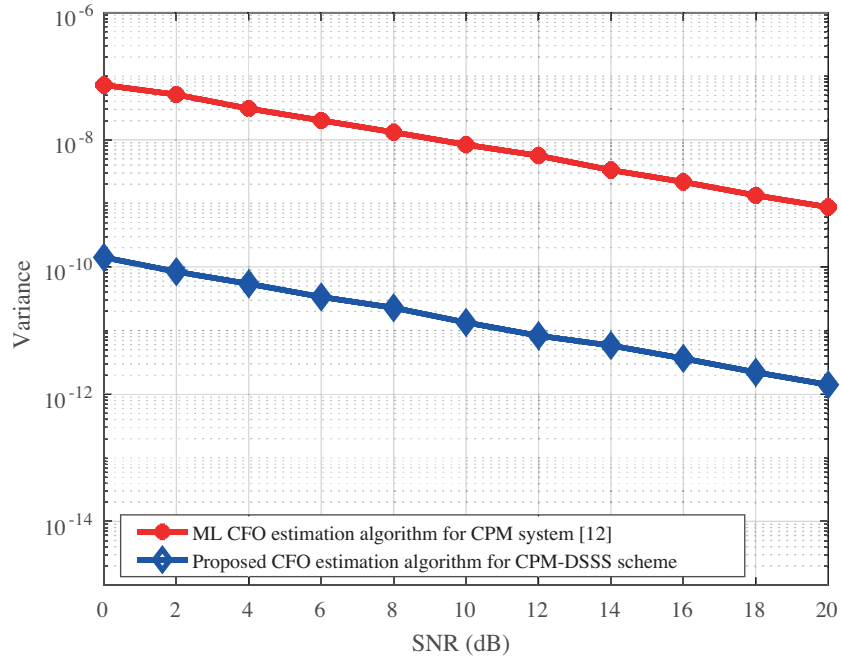


Figure 7. Performance comparison of the proposed CFO estimator algorithm for CPM-DSSS scheme with ML CFO estimator algorithm for CPM system [12].

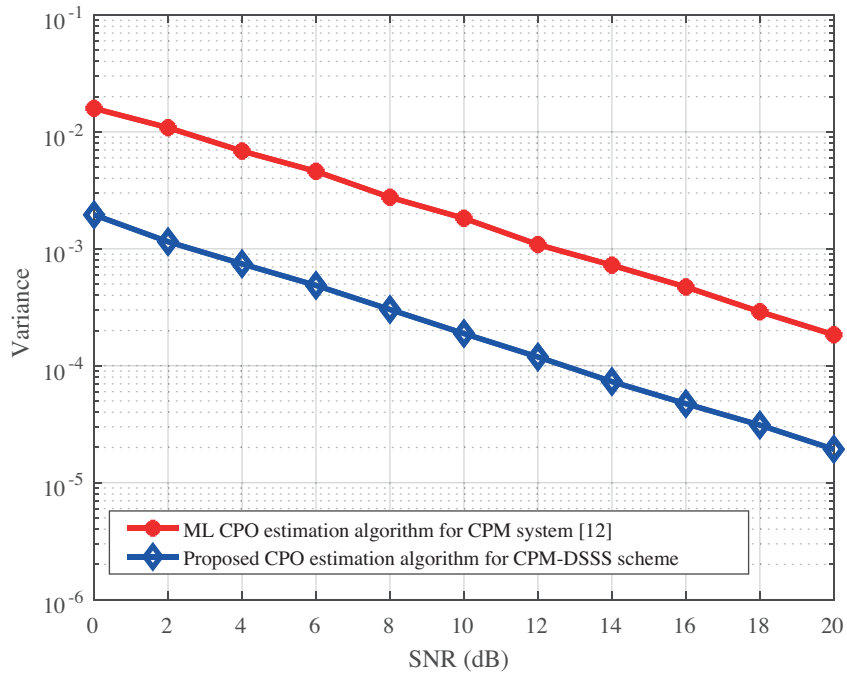


Figure 8. Performance comparison of the proposed CPO estimator algorithm for CPM-DSSS scheme with ML CPO estimator algorithm for CPM system [12].

and additions $\{(L_0 L_c N K_z / 2) \log_2(L_0 L_c N K_z)\}$. Similarly, the computational complexity of Equation (13) for

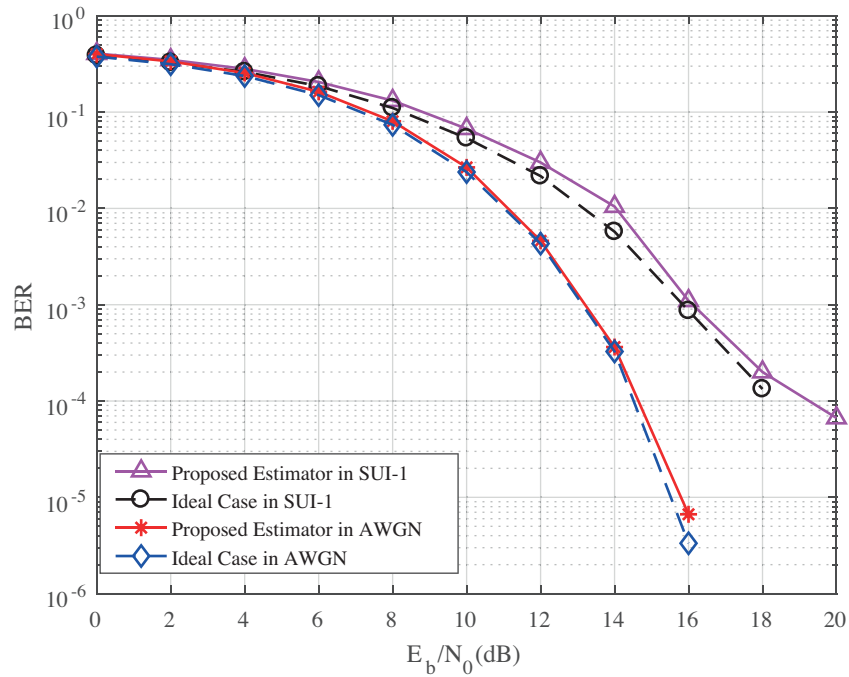


Figure 9. Performance comparison in terms of BER of the proposed joint estimator in AWGN and SUI-1 multipath fading channel with ideal case i.e. when CPO and CFO are known at the receiver.

CPO estimation is given in the Table 1. Finally, for the interpolation equation (15) computational complexity in terms of number of addition/subtraction and multiplication/division can be calculated, including the $v_{\text{resolution}} = \hat{v}_m - \hat{v}_{m-1}$ as shown in the Table 1. If we compare our system computational complexity with [12, 13], because in this work spread sequence is used therefore, our computational complexity is L_c times higher than their system. There is a tradeoff between the system's complexity and performance. Our proposed model is representing a general point-to-point communication system; the worthiness of system performance versus complexity can be decided based on the application by the system's user. For example, if we consider the point-to-point tactical communication, which needs more accuracy and a high level of security, this scheme can be more suitable. Nevertheless, by using the proposed joint estimation algorithm for CPM-DSSS scheme, variance of the estimator is decreased tremendously, as shown in Figures 7 and 8.

5. Conclusion

Our study has devised a joint estimation of CFO and CPO for a hybrid CPM-DSSS scheme. The transmission in the form of bursts is considered. The proposed algorithm is utilized at the receiver to estimate the CFO and CPO from the synchronization preamble of the CPM-DSSS burst. The robustness of our proposed scheme is also tested for the SUI-I multipath fading channel. The results show that although SUI-I is a multipath fading channel but still our proposed estimation algorithm performance is reaching close to AWGN channel.

Moreover, the simulation results presented in this paper are only for binary full response cases; however, to estimate CFO and CPO for binary partial response cases, this work can be extended in future work.

References

- [1] Kar UN, Sanyal DK. An overview of device-to-device communication in cellular networks. *ICT Express* 2018; 4 (4): 2405-9595. doi:10.1016/j.icte.2017.08.002
- [2] Pöpper C, Strasser C, Čapkun S. Jamming-Resistant Broadcast Communication without Shared Keys. In: *Proceedings of the 18th Conference on USENIX Security Symposium*; Montreal, Canada; 2009. pp. 231–248.
- [3] Jenkins SN, Kenney BA, Majid AJ, Moradi H, Farhang-Boroujeny B. CP- DSSS: A Novel Waveform for Multiple Access in IoT. In: *2020 2nd 6G Wireless Summit (6G SUMMIT)*; 2020. pp. 1-5, doi: 10.1109/6GSUMMIT49458.2020.9083792
- [4] Bensky A .Chapter 11 - Wireless local area networks. In: *Short-range Wireless Communication*. 3rd ed. Newnes, 2019, pp. 273-315. doi:10.1016/B978-0-12-815405-2.00011-7
- [5] Liang Y, Ren J, Li T. Secure OFDM System Design and Capacity Analysis Under Disguised Jamming. *IEEE Transactions on Information Forensics and Security* 2020; 15: 738-752. doi: 10.1109/TIFS.2019.2929449
- [6] Ke Z, Wang S, Eryang Z. Coherent RAKE Receiver for CPM-Based Direct Sequence Spread Spectrum. *Mathematical Problems in Engineering* 2016: 1-7. doi: 10.1155/2016/6971083
- [7] Zeeshan M, Khan SA, Mehtab Z. Data aided algorithm for burst detection in wideband networking waveform with FPGA implementation on SDR platform. In: *2014 11th Annual High Capacity Optical Networks and Emerging/Enabling Technologies (Photonics for Energy)*; 2014. pp. 154-158. doi: 10.1109/HONET.2014.7029381
- [8] Asano DK, Hayashi T, Kohno R. Modulation and processing gain tradeoffs in DS-CDMA spread spectrum systems. In: *1998 IEEE 5th International Symposium on Spread Spectrum Techniques and Applications-Proceedings. Spread Technology to Africa (Cat. No. 98TH8333)*; 1998. pp. 9-13.
- [9] Mehlan R, Chen Y, Meyr H. A fully digital feedforward MSK demodulator with joint frequency offset and symbol timing estimation for burst mode mobile radio. *IEEE Transactions on Vehicular Technology* 1993; 42 (4): 434-443. doi: 10.1109/25.260769
- [10] Morelli M, Mengali U. Feedforward carrier frequency estimation with MSK-type signals. *Communications Letters, IEEE* 1998; 2: 235-237. doi: 10.1109/4234.709442
- [11] Morelli M, Mengali U. Joint frequency and timing recovery for MSK-type modulation. *IEEE Transactions on Communications* 1999; 47 (6): 938-946. doi: 10.1109/26.771350
- [12] Hosseini E, Perrins E. Maximum likelihood synchronization of burst-mode CPM. In: *2013 IEEE Global Communications Conference (GLOBECOM)*; 2013. pp.1802-1807. doi: 10.1109/GLOCOM.2013.6831335
- [13] Hosseini E, Perrins E. Timing, Carrier, and Frame Synchronization of Burst-Mode CPM. *IEEE Transactions on Communications* 2013; 61(12): 5125-5138. doi: 10.1109/TCOMM.2013.111613.130667
- [14] Hosseini E, Perrins E. Training sequence design for data-aided synchronization of burst-mode CPM. In: *2012 IEEE Global Communications Conference (GLOBECOM)*; 2012. pp.2234-2239. doi: 10.1109/GLOCOM.2012.6503447
- [15] Zeeshan M, KHAN S, HAQ I. A Two Stage Algorithm for Carrier Frequency Offset Recovery with DSP Implementation on SDR Platform. *IEICE Transactions on Communications* 2014;E97.B: 2449-2458 doi: 10.1587/transcom.E97.B.2449
- [16] Lin Q, Mohan S and Weitnauer MA. Interference-insensitive synchronization scheme of MSK for transmit-only Wireless Sensor Network. In: *2016 IEEE International Conference on Communications (ICC)*; 2016, pp. 1-6, doi: 10.1109/ICC.2016.7510855
- [17] Shehzadi S, Sheikh SA, Kulsoom F, Zeeshan M and Khan QU. A Robust Timing and Phase Offset Estimation Technique for CPM-DSSS-Based Secured Communication Link. in *IEEE Access* 2021; 9: 111143-111151. doi: 10.1109/ACCESS.2021.3102308

- [18] Wang C, Cui G, Wang W, Zhang Y. Joint estimation of carrier frequency and phase offset based on pilot symbols in quasi-constant envelope OFDM satellite systems. *China Communications* 2017; 14 (7) : 1-11. doi: 10.1109/CC.2017.8019135
- [19] Kulsoom F, Vizziello A, Borra R, Savazzi P. Reduced complexity Kalman filtering for phase recovery in XPIC systems. *Physical Communication* 2018; 29 : 112-119.
- [20] Golay M. Complementary series. *IRE transactions on information theory* 1961; 7 (2): 82-87.
- [21] Abdullah SSBS, Khalifa OO, Rahman FA, Nasir H. Performance Evaluation on Error Probabilities of Coded BPSK System Using the Linear (23, 12) Golay Code with Hard-Decision Decoding. In: 2019 IEEE International Conference on Smart Instrumentation, Measurement and Application (ICSIMA); 2019 .pp. 1-4. doi: 10.1109/IC-SIMA47653.2019.9057337
- [22] Shahzad K, Gulzar S, Khan Shoab. A novel hybrid narrowband/wideband networking waveform physical layer for multiuser multiband transmission and reception in software defined radio. *Physical Communication* 2019; 36: 100790. doi: 10.1016/j.phycom.2019.100790
- [23] Zeeshan M, Khan SA. A robust carrier frequency offset estimation algorithm in burst mode multicarrier CDMA based ad hoc networks. *International Journal of Communication Networks and Information Security* 2012; 4 (3): 174.
- [24] Erceg V, Hari KVS, Smith M, Baum D, Sheikh K, Tappenden C et al. Channel Models for Fixed Wireless Application. IEEE 802.16 Broadband Wireless Access Working Group, Tech Rep 2001. [Online]. Available: https://www.researchgate.net/publication/243777280_Channel_Models_for_Fixed_Wireless_Application
- [25] Zeeshan M, Khan Shoab. Robust Sampling Clock Recovery Algorithm for Wideband Networking Waveform of SDR. *International Journal of Communication Networks and Information Security* 2013; 5 (1): 10-18.
- [26] Mengali U. Synchronization techniques for digital receivers. Springer Science & Business Media, 2013.
- [27] Oppenheim AV, Schafer RW. Discrete-time signal processing. Pearson Education, 2010.